RSC Advances

PAPER

View Article Online
View Journal | View Issue

Cite this: *RSC Adv.*, 2021, **11**, 28573

Efficient nickel or copper oxides decorated graphene–polyaniline interface for application in selective methanol sensing†

Nhat Xuan An Nguyen,[a] Le Viet Hai,*[a] Thi Kim Ngan Nguyen,[a] Thi Nam Pham,[b] Thi Thom Nguyen,[b] Le Thanh Nguyen Huynh,[a] Van Viet Pham,[a] Thi Thu Trang Nguyen ,[b] Nguyen Thai Hoang[a] and Tran Dai Lam *[bc]

Received 29th May 2021
Accepted 26th July 2021

DOI: 10.1039/d1ra04164a

rsc.li/rsc-advances

Graphene sheets decorated with nickel or copper oxides that were anchored on polyaniline (denoted as PANI-graphene/NiO and PANI-graphene/CuO) were prepared by a simple, easy to-control electrochemical method and applied as novel materials for sensitive and selective methanol sensing. The fabricated sensors exhibited good electrocatalytic activity, appropriate dynamic linear range (20–1300 mM), sensitivity (0.2–1.5 μA mM^{-1} cm^{-2}) and excellent selectivity towards methanol. It should be highlighted from the selectivity tests that no significant interference was observed from ethanol and other alcohols. To our best knowledge, using inexpensive but efficient transition metals like Ni, Cu instead of Pt, Pd and their composites with PANI, graphene would be scientifically novel and practically feasible approach for sensor fabrication that could be potentially used to identify methanol adulteration in counterfeit alcoholic beverages.

1. Introduction

Methanol (MeOH) is one of the most widely used organic solvents in industrial and household products as well as one of the most potential candidates for an alternative automobile fuel.[1] Compared to ethanol (EtOH), MeOH is less expensive and more easily available, thus it could be accidentally sold or intentionally added to beverages to strengthen the effects of alcohol for more profit. Moreover, it could be abused as a substitute for EtOH fuel. This could be very dangerous, as MeOH was known for its toxicity to human health and its metallic corrosion, especially towards aluminum (the most used metal in manufacturing vehicles). According to the US Occupational Safety and Health Administration, 8 hour Time Weighted Average (TWA) and Short-Term Exposure Limit (STEL) for MeOH was 200 ppm and 250 ppm, respectively.[2] Considering the harmful effects of MeOH, this requires good measures to determine its permitted levels in the use of chemical, fuel, and food industry.

Development of a simple/economical, but sensitive/selective as well as practical/label-free method is essentially demanded for environmental monitoring, food industry and clinical diagnostics.[3,4] Traditional methods for the quantitative analysis of MeOH including chromatography – mass spectrometry (GC-MS), gas chromatography – flame ionization detector (GC-FID), headspace – gas chromatography (HS-GC), however, these methods required the complex and expensive apparatus, and therefore incompatible for practical routine monitoring of MeOH.[5] Over the past decade, MeOH sensors have been proposed as an alternative method for MeOH detection due to their rapid response, low cost, and portability.[5–7] These sensors can be classified into two groups based on the mechanism of operation including physical (density, capacitance, viscosity, sound velocity, infrared/Raman spectroscopy, refractive index, heat capacity) and electrochemical types. The low selectivity of the physical sensors linked to similarity in physical properties of alcohols has limited their application. Otherwise, the (electro)chemical sensors offer many advantages thank to their electrical output signal, sensibility, and selectivity. So far, most electrochemical MeOH sensors are developed based on the operating characteristics of the liquid-fed direct MeOH fuel cells (DMFCs). These fuel cell type sensors are very useful for monitoring the concentration of MeOH in the DMFCs. However, this remains extremely difficult for other applications such as the analysis of MeOH in beverages and fuels. While the other approach based on enzyme-modified electrodes (biosensors) remains the challenge of low selectivity as well as stability. Therefore, it is essential to develop simpler and more practical techniques for directly detecting MeOH in the liquid phase.

[a]*HCM City University of Science, Vietnam National University HCM City, 227 Nguyen Van Cu, HCM City, Vietnam. E-mail: lvhai@hcmus.edu.vn*

[b]*Institute for Tropical Technology, Vietnam Academy of Science and Technology, 18 Hoang Quoc Viet, Hanoi, Vietnam. E-mail: tdlam@itt.vast.vn*

[c]*Graduate University of Science and Technology, Vietnam Academy of Science and Technology, 18 Hoang Quoc Viet, Hanoi, Vietnam*

† Electronic supplementary information (ESI) available. See DOI: 10.1039/d1ra04164a

In this context, the development of non-enzymatic electrochemical sensors using various materials including polymers,[8,9] metal[10] and metal oxide[11–14] nanoparticles (NPs), carbon-based materials and their composites[12,15–17] has been intensively explored. In particular, metal and metal oxide NPs, such as Pt,[18] Cu,[19,20] CuO,[11,21] and Pd[22] NPs, have attracted significant attention because of their high surface energy and large surface area and thus high electrochemical catalytic activity in numerous electrochemical processes, including methanol electrooxidation. Normally, these NPs are loaded onto the inorganic/organic supports as electrochemical catalysts. It is of crucial importance to ensure both even dispersion and good electron transfer between the surface of NPs and electrode to get higher sensitivity and lower detection limit. Typically, some inorganic–inorganic, organic–organic, inorganic–organic configurations have been proposed such as palladium–nickel/silicon nanowires (Pd–Ni/SiNWs);[22] NiO/Fe_2O_3;[23] Au–Ni/graphene oxide;[24] graphene–NiO nano composites;[25] polymethyl methacrylate–graphene–carbon nanotubes;[26] reduced graphene oxide/ferricyanide;[27] *N*-5-methoxysalicylaldehyde, *N*′-2-hydroxyacetophenone – 1,2 phenylenediimino nickel(II) (Ni(II)–MHP) and reduced graphene oxide (RGO) (Ni(II)–MHP/RGO);[28] EG/rGO/np–NiOOH;[29] PTh-α-Fe_2O_3 [30]… Although Pt and Pt-based catalysts are common and efficient for MeOH oxidation, there are some significant obstacles preventing their large-scale application such as high cost, reactivity, and the extent of poisoning towards MeOH.

Primary objective of this work is to construct nanocomposite of PANI–graphene to get the appropriate sensitivity, higher selectivity (against other alcohols) for MeOH determination. Despite polyaniline (PANI) is among one of the most widely investigated conductive polymers because of its interesting redox properties, high stability and ease of preparation and graphene is considered as one of the most interesting materials due to its excellent characteristics including its high conductivity. On the other hand, graphene is well-known as a planar sp^2 carbon nanostructure that could render the high surface area, outstanding electrical, thermal, and mechanical properties. Moreover, using less expensive but equally efficient transition metals like Ni, Cu instead of Pt, Pd and their composites with PANI, graphene should be also a much more promising approach. For these reasons, PANI–graphene/NiO (or CuO) platforms can be foreseen with following advantageous features: (i) PANI–graphene is capable of eliminating the main drawbacks of the electrochemical sensors such as the phenomenon of "electrode fouling" or "memory effect" from one sample to another as well as the possibility to be produced inexpensively and controllably at large scale; (ii) PANI–graphene interface is expected to express a synergic effect to the overall system and thus improve sensing characteristics; and (iii) the enhanced oxidation of MeOH is likely to occur more favorably at PANI–graphene/NiO (or CuO) compared to that of other alcohol interferences, making the MeOH sensor highly selective and electrochemically feasible. According to the available literature, to the best of our knowledge there is no previous report on the design of PANI–graphene, NiO or CuO catalyzed electrodes for electrochemical detection of liquid methanol from the alcohol mixtures.

2. Experimental

2.1. Chemicals and apparatus

Aniline (ANI) was obtained from ACROS Organics™ and was purified before use. Analytical-grade graphene (Production code: ANT-GNPs-160101, bulk density of 0.015 g mL^{-1}, diameter of 10–20 μm, thickness <5 nm, C content ≥99%) were purchased from Applied Nano Technology Joint Stock Company (ANTECH, Vietnam). $CuCl_2 \cdot 2H_2O$ (99%) and $NiCl_2$ (98%) were obtained from Acros Organics. Sodium hydroxide (NaOH, 98%), methanol (MeOH, 99.9%), ethanol (EtOH, 99%), isopropyl alcohol (IPA), acetone, sulfuric acid (H_2SO_4, 99%) were supplied by Fisher, Scientific. Electrochemical experiments were on Gamry Interface 1010T system, using a FTO working electrode (resistance of 8 Ωm cm^{-1}, thickness of 2.2 mm, Dyesol, Australia), with a platinum sheet as the counter electrode, and Ag/AgCl in 3.5 M KCl electrode as the reference. Fourier transform infrared spectra (FTIR) were collected with Bruker LUMOS II; field-emission scanning electron microscopic (FE-SEM) and high resolution transmission electron microscopic images were analyzed using JEOL JSM-6480LV and Multipurpose 200 kV JEM 2100 JEOL respectively; energy-dispersive X-ray spectroscope (EDS) was obtained with Hitachi SU-8010; Raman spectrometer was collected using Jobin Yvon Labram 300; X-ray diffractometer was done with D8 Advance Eco, Bruker.

2.2. PANI–graphene/NiO, PANI–graphene/CuO electrode fabrication

The sensing electrodes were fabricated by cyclic voltammetry (CV) using the FTO as conducting substrate. The FTO glasses were cleaned with distilled water and ethanol in an ultrasonic bath and dried at 120 °C before electrochemical experiments. The electrode preparation protocol comprising three main steps. Firstly, the electrodeposition PANI–graphene films were carried out using the CV method with scanning potentials between −0.5 V and 1.3 V for 20 cycles at a scan rate of 30 mV s^{-1}. The electrolyte containing 0.1 M aniline, and 0.5 M H_2SO_4 in a mixture of H_2O/IPA (v/v = 1/1) has previously dispersed graphene by sonication (0.01 mg mL^{-1}). After 20 CV cycles, the PANI–graphene coated FTO (FTO/PANI–graphene) was rinsed with deionized water, EtOH, and then leave for dried at room temperature. For comparison, PANI film was also prepared using the same protocol as PANI–graphene. Secondly, metal catalyst (Ni, Cu) was electrodeposited onto the FTO/PANI–graphene electrodes from a solution of 0.025 M $CuCl_2 \cdot 2H_2O$ (or 0.025 M $NiCl_2$) in KCl 0.1 M aqueous electrolyte solution by the CV method (potential range of −0.3 to −0.9 V, 20 cycles, scan rate of 100 mV s^{-1}). The modified electrodes were then rinsed with deionized water then allowed to dry at room temperature before electrooxidation step. Finally, the surface functionalized metals (Ni, Cu) were electrooxidized to their respective oxides (NiO, CuO) in 0.1 M NaOH electrolyte by CV method (potential range from 0 to 0.8 V, 5 cycles, scan rate of 50 mV s^{-1}). The films were rinsed with deionized water then allowed to dry at room temperature to obtain FTO/PANI–graphene/NiO and FTO/PANI–graphene/CuO sensing electrodes.

2.3. Characterization of methanol sensor

Electrocatalytic oxidation of MeOH on the sensing electrodes (FTO/PANI–graphene/NiO, FTO/PANI–graphene/CuO) were examined in a 0.1 M NaOH solution containing 50 mM methanol by CV method (potential range of 0 to 1.3 V, scan rate of 100 mV s^{-1}). The detection performance of the sensors was studied by the chronoamperometry (CA) method at an applied potential of 0.55 V in a 0.1 M NaOH electrolyte with constant stirring and successive addition of methanol up to 1500 mM. The selectivity of the sensor was tested by the CA method using different alcohols (EtOH, IPA, acetone). Further, the sensing electrodes were also analyzed with real samples using alcoholic distilled beverages.

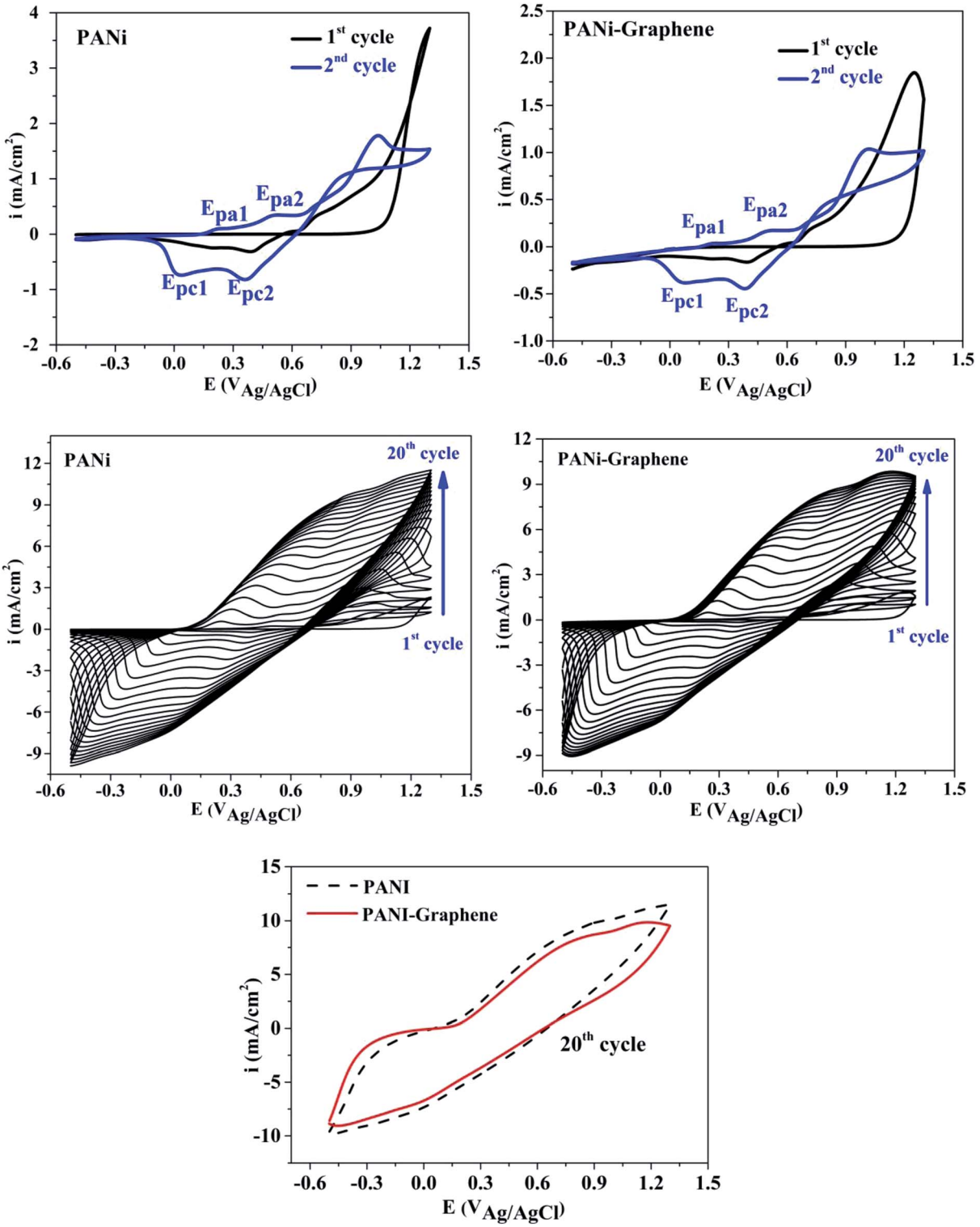

Fig. 1 CV curves during electropolymerization of PANI and PANI–graphene.

3. Results and discussion

3.1. Electrochemical synthesis of PANI–graphene

Fig. 1 shows the cyclic voltammograms during the electropolymerization of PANI and PANI–graphene. The anodic peak appeared in the first scan was ascribed to the oxidation of ANI. From the second scan, this ANI oxidation peak was overlapped with the oxidation peaks (E_{pa1}, E_{pa2}) of the PANI product deposited on the FTO electrodes.[31] The CVs show that the current density increases in each successive cycle, confirming

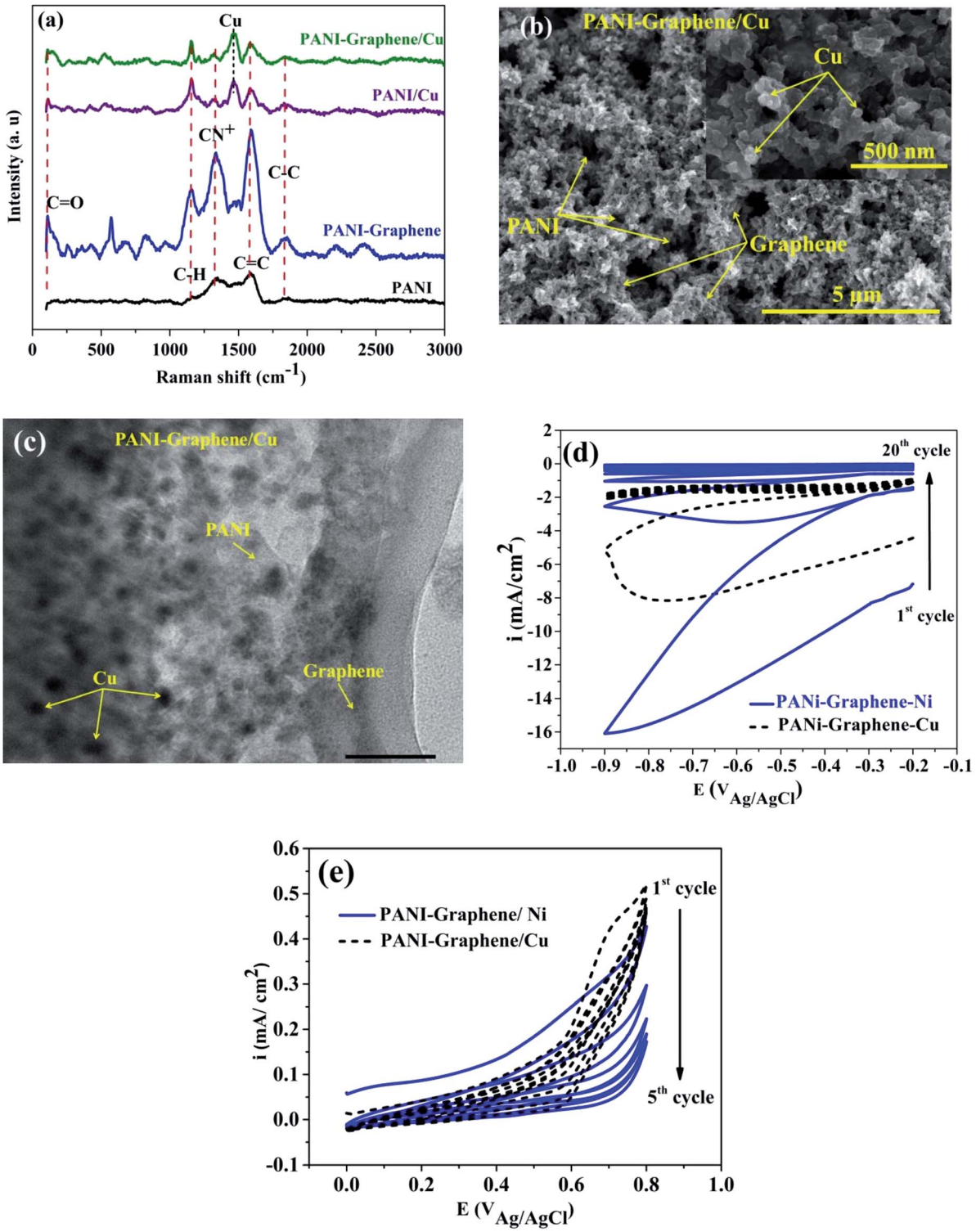

Fig. 2 (a) Raman spectra; (b) SEM image; (c) HRTEM image of PANI–graphene/Cu, and (d and e) CV curves for electrodeposition and electrooxidation of Ni, Cu on PANI–graphene.

electrodepositing, thickening PANI films. It can be additionally seen from Fig. 1 that the redox peaks of the PANI–graphene (sharper) composite are more reversible than those of PANI (broader) which is a result of the highly electrical conductive graphene.

The Raman spectra of the samples exhibit two distinct peaks at around 1350 and 1590 cm^{-1} corresponding to the well-defined D band and G band, respectively (Fig. 2a). The graphitic peak (G band at 1590 cm^{-1}) is due to the E_{2g} vibrational mode of the C–C bond stretching and the disorder peak (D-band at 1350 cm^{-1}) is due to the A_{1g} vibrational mode. The intensity ratio of the D and G bands (I_D/I_G ~0.93) allows to estimate the defects of graphene where a lower ratio ensures less defects on graphene. Moreover, from Raman spectra, it can be expected that a strong interaction between PANI and graphene will facilitate effective degree of electron delocalization, and thus enhance electron transfer and the selectivity of electrochemical detection with PANI/graphene interface compared to that of pure PANI. Logically, Raman spectra intensity was weaker for PANI–graphene/CuO (or NiO), after subsequent electrodeposition and electrooxidation. SEM images confirmed high porous structure of PANI–graphene, which is important for Ni (or Cu) occupancy after the electrodeposition (Fig. 2b). Further HRTEM images showed that the Ni or Cu nanoparticles were successfully incorporated onto PANI–graphene nanocomposites (Fig. 2c). The existence of graphene in porous structure can provide a larger specific surface area than pure PANI. The next steps of electrodeposition/oxidation of Ni/NiO (or Cu/CuO) on the surface of PANI–graphene (Fig. 2d and e) were also visualized and compared by FTIR, XRD, EDX analyses of PANI, PANI–graphene and PANI–graphene/NiO (or CuO) composites (Fig. S1–S3, Table S1, ESI†). In summary, on the basis of the above characterization results, it can be concluded that: (i) graphene facilitated electron transport on the electrode surface; (ii) the porous framework of PANI–graphene can be beneficial for Ni or Cu electrodeposition as well the enhanced electron transfer throughout the interface; (iii) enhanced oxidation of MeOH should be expected on synergic PANI–graphene/NiO (or CuO) platform.

3.2. MeOH electrooxidation

Fig. 3 indicated that PANI in PANI–graphene/CuO, being not in acid doped form, are not electroactive in alkaline solution (black line). In the alkaline solution containing MeOH or EtOH, a new peak appeared in anodic scan at about 0.8–0.85 V, which was attributed to the MeOH and EtOH oxidation that did take place after the oxidation of NiO/CuO to NiOOH/CuOOH, according to the following reactions:[32–34]

$$CuO/NiO + OH^- \rightarrow CuOOH/NiOOH + e \quad (1)$$

$$CuOOH/NiOOH + MeOH + 3O_2 \rightarrow CO_2 + Cu(II) + 4H_2O \quad (2)$$

It is well known that the electrooxidation processes of MeOH and EtOH are very similar to each other and are kinetically slow. From the CV curves, it can be seen that the oxidation potential peak of MeOH (E_{peak} at 0.8 V) is slightly lower than that of EtOH (E_{peak} at 0.85 V), but the respective current intensity of the former is much higher than that of the later. Significantly higher peak current densities recorded with MeOH clearly demonstrated the importance of NiO/CuO in MeOH electrooxidation (the electroactivity difference between PANI–graphene and PANI–graphene/CuO in alkaline medium was compared in Fig. S4†). Theoretically, to obtain the highest signal (the largest current), the applied potential in chronoamperometry should be fixed at MeOH oxidation peak potential (0.8 V), however, to deliberately eliminate the involved process of EtOH (to have the best signal/noise), the chronoamperometric curves were recorded at lower onset oxidation potential (0.55 V).

3.3. MeOH selectivity detection

To investigate the selectivity of PANI-graphene/NiO (or CuO) films towards MeOH, the experiments were done for a series of other alcohols such as EtOH, IPA, acetone. As discussed above, to get the best signal/noise (best MeOH selectivity with the lowest oxidation of interferents), the chronoamperometric curves were taken at the onset oxidation potential (0.55 V).

Some important remarks could be drawn from Fig. 4. First, both PANI–graphene/NiO and PANI–graphene/CuO had no response to all added interferences, including EtOH (50 mM added). The electrooxidation of MeOH was significant compared to that of other interferences (EtOH, IPA, acetone): the current intensity for MeOH oxidation (added 50 mM, i ~3.5 μA cm^{-2}) was greater than that of other interferences at high concentration (200 mM, i < 0.5 μA cm^{-2}). It could be supposed that the detection of MeOH was quite selective even at high concentration of interferences (Fig. S5, ESI†).

Next, since Ni/NiO particles were electrodeposited in a greater quantity on PANI–graphene compared to that of Cu/CuO (see Fig. 2d: the reduction current of the first cycles during metallic electrodeposition), the MeOH oxidation on

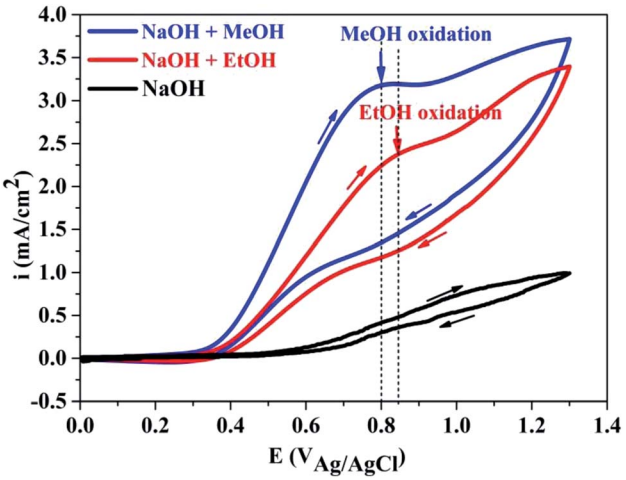

Fig. 3 The electrooxidation of MeOH 50 mM, EtOH 50 mM on PANI–graphene/CuO.

PANI–graphene/NiO should be more sensitive compared to that on PANI–graphene/CuO for a low MeOH concentration range, as it was experimentally confirmed from the slope values of calibration plots (Fig. 4d, for concentration below 100 ppm). At higher MeOH concentration range, the response currents of PANI–graphene/NiO and PANI–graphene/CuO resembled each other, confirming the same sensitivity for Cu and Ni in that concentration range. The similar electrocatalytic of Ni and Cu in MeOH oxidation can be explained by their similarities in the crystallographic data (both with the same face centered cubic (fcc) structure and lattice parameters) and surface properties. Furthermore, the calibration plots displayed two different slopes related to two linear zones, corresponding to two different ranges of MeOH concentrations: (i) lower concentration from 0 to 400 ppm and (ii) higher concentration from 400 to 1300 ppm, in which the sensitivity decline observed at higher MeOH concentration is likely related to the saturation of the electrocatalytic active sites with MeOH target molecules. The main electroanalytical parameters obtained from different MeOH sensors were compared and summarized in Table 1.

To determine the practical performance and feasibility of the above sensor, the determination of MeOH from real samples of alcoholic beverage was examined. Taking into account the fact that Cu was almost two times cheaper than Ni, PANI–graphene/CuO was chosen for further evaluations with real samples. The results were summarized in Table 2. The recoveries of the samples were in range of 85–99%, indicating that the detection procedure can be used as an effective electrochemical determination of MeOH in the commercial samples.

Table 1 Analytical parameters obtained from different MeOH sensors

Sensor interfaces	Range (mM)	Sensitivity ($\mu A\ mM^{-1}\ cm^{-2}$)	Ref.
PANI–graphene/NiO	20–100	1.5	This work
	300–1300	0.2	
PANI–graphene/CuO	20–300	0.8	This work
	300–1300	0.2	
EG/rGO/np-NiOOH	10–40	1.32	29
Graphene/NiO/GCE	0.2–24	2.21	25
Pd–Ni/SiNWs	0–75	1.96	22
PMMA–graphene–CNTs	1×10^{-6} to 10	13.494	26
PTh-α-Fe_2O_3/GCE	5–1000	0.793	30
Pt/CNTs	25–100	6	11

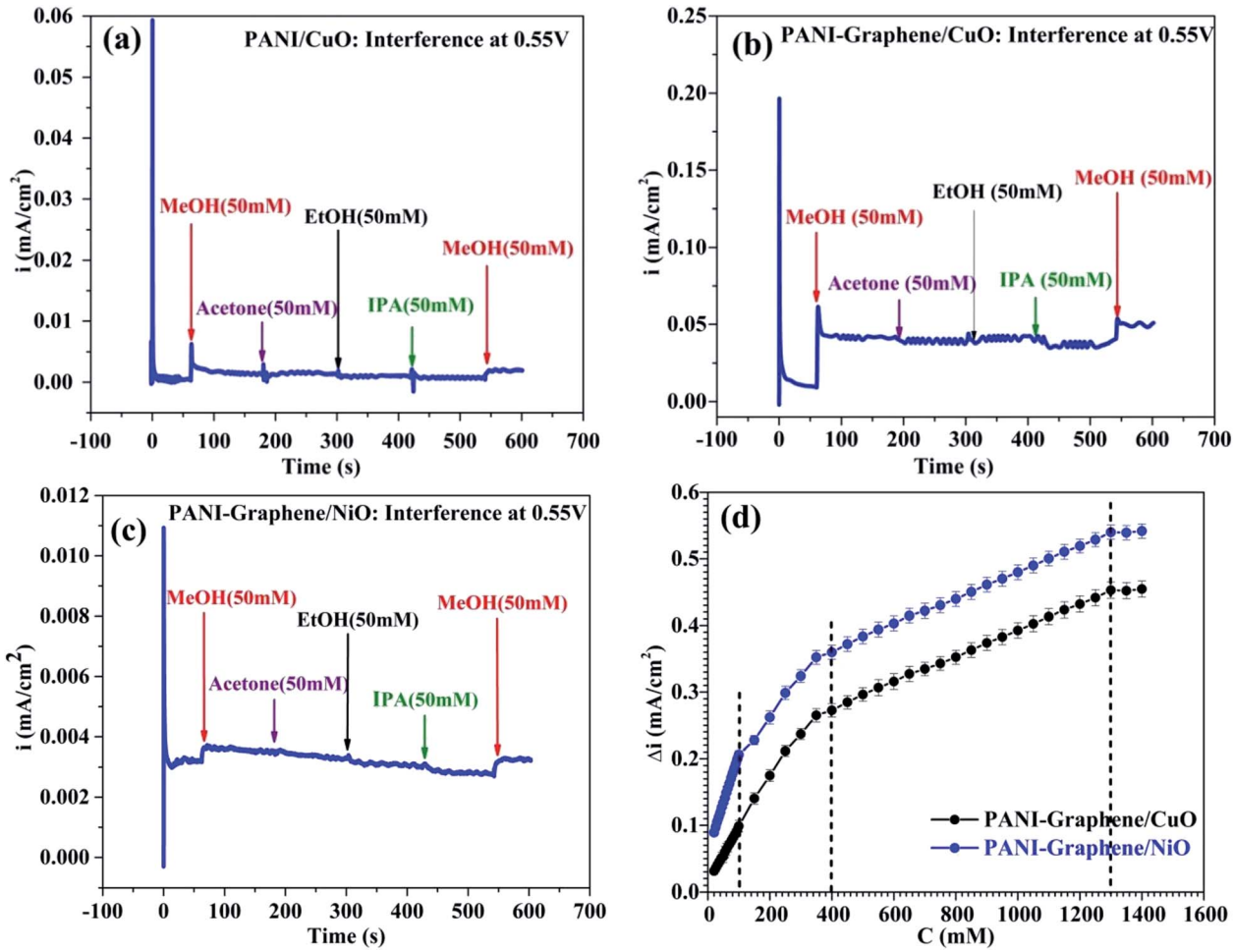

Fig. 4 MeOH selectivity *vs.* EtOH and other interferents: (a) PANI/CuO; (b) PANI–graphene/CuO; (c) PANI–graphene/NiO sensor electrodes; (d) the calibration curves of PANI–graphene/NiO and PANI–graphene/CuO sensor electrodes.

Table 2 Determination of MeOH in real samples using PANI-graphene/CuO

Parameter	S1	S2	S3
0.1 M NaOH volume (mL)	30	30	30
Added real sample (mL)	6	6	6
MeOH conc. (ppm) in real sample	2500	3700	4900
Diluted MeOH conc.[a] (ppm) in electrochemical cell test	416.6	616.6	816.6
MeOH found[b] (ppm) (before diluted of real sample)	2479	3187	4175
Recovery (%)	99	86	85

[a] Value was obtained by the appropriate dilution factor equal 1/6. [b] Average of three replicates.

4. Conclusion

PANI–graphene/NiO and PANI–graphene/CuO based MeOH sensor with appropriate linear response range, sensitivity, good reproducibility, selectivity, and long-time stability was expected to meet the requirements of real sample detection of smuggled alcoholic beverages whose illegal production/consumption is quite popular in many developing countries. One advantageous aspect of this sensor is its low cost and its ability to detect MeOH selectively from binary MeOH–EtOH, and therefore, may be of great importance for authorities to consider the necessary measures and legal acts preventing smuggled commerce and reducing toxicity risk of methanol.

Conflicts of interest

The authors declare that they have no known competing financial interests or personal relationships that could have appeared to influence the work reported in this paper.

Acknowledgements

The work was supported by Department for Science and Technology of Ho Chi Minh City (114/2019/HĐ-QPTKHCN).

References

1 D. S. Islek and S. Ramadanoglu, *Med. Sci.*, 2017, **6**(2), 372–374.
2 H. Ghorbani, A. Nezami, B. Sheikholeslami, A. Hedjazi and M. Ahmadimanesh, *J. Occup. Med. Toxicol.*, 2018, **13**, 8.
3 H.-J. Chun, J. L. Poklis, A. Poklis and C. E. Wolf, *J. Anal. Toxicol.*, 2016, **40**, 653–658.
4 N. Shoaie, M. Daneshpour, M. Azimzadeh, S. Mahshid, S. M. Khoshfetrat, F. Jahanpeyma, A. Gholaminejad, K. Omidfar and M. Foruzandeh, *Microchim. Acta*, 2019, **186**, 465.
5 H. Zhao, J. Shen, J. Zhang, H. Wang, D. P. Wilkinson and C. E. Gu, *J. Power Sources*, 2006, **159**, 626–636.
6 J. van den Broek, S. Abegg, S. E. Pratsinis and A. T. Güntner, *Nat. Commun.*, 2019, **10**, 4220.
7 A. Genner, C. Gasser, H. Moser, J. Ofner, J. Schreiber and B. Lendl, *Anal. Bioanal. Chem.*, 2017, **409**, 753–761.
8 C. C. Mayorga-Martinez, Z. Sofer and M. Pumera, *Angew. Chem., Int. Ed.*, 2015, **54**, 14317–14320.
9 H. Zhao, J. Shen, J. Zhang, H. Wang, D. P. Wilkinson and C. E. Gu, *J. Power Sources*, 2006, **159**, 626–636.
10 D.-S. Park, M.-S. Won, R. N. Goyal and Y.-B. Shim, *Sens. Actuators, B*, 2012, **174**, 45–50.
11 D. Meng, S. Zhang, T. Thomas, C. Huang, J. Zhao, R. Zhao, Y. Shi, F. Qu and M. Yang, *Sens. Actuators, B*, 2020, **307**, 127686.
12 W. Sun, G. Sun, W. Yang, S. Yang and Q. Xin, *J. Power Sources*, 2006, **162**, 1115–1121.
13 M. Rashid, T.-S. Jun, Y. Jung and Y. S. Kim, *Sens. Actuators, B*, 2015, **208**, 7–13.
14 Y.-G. Zhou, J.-J. Chen, F. Wang, Z.-H. Sheng and X.-H. Xia, *Chem. Commun.*, 2010, **46**, 5951–5953.
15 M. S. Hosseini, S. Zeinali and M. H. Sheikhi, *Sens. Actuators, B*, 2016, **230**, 9–16.
16 W. A. El-Said, M. A. AlMalki, E. M. Sayed, D. A. El-Hady and W. Alshitari, *Mater. Lett.*, 2020, **279**, 128498.
17 K. S. Bhavani, T. Anusha and P. K. Brahman, *Int. J. Hydrogen Energy*, 2019, **44**, 25863–25873.
18 B. Chokkiah, M. Eswaran, S. M. Wabaidur, Z. A. Alothman, P.-C. Tsai, V. K. Ponnusamy and R. Dhanusuraman, *Fuel*, 2020, **279**, 118439.
19 M. S. Shivakumar, G. Krishnamurthy, C. R. Ravikumar and A. S. Bhatt, *J. Sci.: Adv. Mater. Devices*, 2019, **4**, 290–298.
20 B. Tao, J. Zhang, S. Hui, X. Chen and L. Wan, *Electrochim. Acta*, 2010, **55**, 5019–5023.
21 D. P. Quan, B. T. P. Thao, N. V. Trang, N. L. Huy, N. Q. Dung, M. U. Ahmed and T. D. Lam, *J. Electroanal. Chem.*, 2021, **893**, 115322.
22 A. K. Das, N. H. Kim, D. Pradhan, D. Hui and J. H. Lee, *Composites, Part B*, 2018, **144**, 11–18.
23 B. Tao, J. Zhang, S. Hui, X. Chen and L. Wan, *Electrochim. Acta*, 2010, **55**, 5019–5023.
24 S. Jana, A. Mondal and A. Ghosh, *Appl. Catal., B*, 2018, **232**, 26–36.
25 Y. Zhang, Y. Song, J. Zhao, S. Li and Y. Li, *J. Alloys Compd.*, 2020, **822**, 153322.
26 M. M. Rahman, M. A. Hussein, K. A. Alamry, F. M. Al Shehry and A. M. Asiri, *Talanta*, 2016, **150**, 71–80.
27 K. Subbiah, N. Nesakumar, A. J. Kulandaisamy and J. B. B. Rayappan, *Sens. Actuators, B*, 2017, **248**, 708–717.
28 A. Benvidi, M. D. Tezerjani, A. D. Firouzabadi, M. Rezaeinasab, M. M. Ardakani, A. H. Kianfar and M. Sedighipoor, *J. Chin. Chem. Soc.*, 2018, **65**, 603–612.

29 J. P. J. de Oliveira, M. B. S. Emeterio, A. C. de Sá, L. L. Paim and M. del Valle, *Proceedings*, 2019, **42**, 5.
30 F. A. Harraz, M. Faisal, M. Jalalah, A. A. Almadiy, S. A. Al-Sayari and M. S. Al-Assiri, *Appl. Surf. Sci.*, 2020, **508**, 145226.
31 L. D. Tran, D. T. Nguyen, B. H. Nguyen, Q. P. Do and H. Le Nguyen, *Talanta*, 2011, **85**, 1560–1565.
32 S.-J. Li, N. Xia, X.-L. Lv, M.-M. Zhao, B.-Q. Yuan and H. Pang, *Sens. Actuators, B*, 2014, **190**, 809–817.
33 D. W. Kim, J. S. Lee, G. S. Lee, L. Overzet, M. Kozlov, A. E. Aliev, Y. W. Park and D. J. Yang, *J. Nanosci. Nanotechnol.*, 2006, **6**, 3608–3613.
34 M. Karimzadeh, K. Niknam, N. Manouchehri and D. Tarokh, *RSC Adv.*, 2018, **8**, 25785–25793.